

# EVALUATION OF THE EFFECT OF FILTERS ON RECONSTRUCTED IMAGE QUALITY FROM CONE BEAM CT SYSTEM

B. N. Ha<sup>[1]</sup>, B. T. Hung<sup>[1]</sup>, T. T. Duong<sup>[1]</sup>, T. K. Tuan<sup>[1]</sup>, T. N. Toan<sup>[2]</sup>

1. Hanoi University of Science and Technology

2. Vietnam Atomic Energy Institute

Email: ha.buingoc@hust.edu.vn

**Abstract:** 3D Filtered Back Projection (FBP) is a three-dimensional reconstruction algorithm usually used in Cone Beam Computed Tomography (CBCT) system. FBP is one of the most popular algorithms due to its simplicity. FBP can produce 3D reconstructed objects much quicker. It can also handle a more considerable amount of data while not requiring powerful computer hardware than other algorithms. The quality of a reconstructed image by the FBP algorithm strongly depends on spatial filters and denoise filters applied to projections. This paper will evaluate the reconstructed image quality of the CBCT system by using different denoise filters and spatial filters and then finding out the best filters for the CBCT system.

**Keyword:** Cone-Beam CT, FBP, Filter, Reconstruction

## I. INTRODUCTION

Cone-Beam Computed Tomography (CBCT) is a transmission tomography technic that was invented by Godfrey N. Hounsfield in 1967. CBCT was first used in medical imaging diagnostic in 1990 [1]. In recent years, CBCT has been increasingly used in None-Destruction Testing (NDT), industrial object metrology [3,4]. The development of radiation detection, mechanical engineering, and information technology made CBCT technic have remarkable improvement, such as increasing image contrast and having higher spatial resolution of the reconstructed Object.

Today, the modern CBCTs usually use an X-ray generator with a focal spot size of only around a few micrometers. Flat Panel Detector has a pixel size from several dozen to smaller than 200 micrometers. This configuration allows CBCT to scan and produce reconstructed images with a spatial resolution up to several micrometers, making modern CBCT inspect and measure the very fine and complex samples' structure. CBCT has been commonly used for industrial applications in the inspection and metrology of models such as casting objects, plane's components, electronic printed board, and lithium battery. With the ability to penetrate the Object, CBCT allows to analyze material density, inspect none surface defect that cannot be performed by other scanning methods [2,4].

Follow the improvement of CBCT's hardware; reconstruction algorithms have been quickly developed to produce reconstructed images with higher quality, reduce reconstruction time. There are several algorithms that are usually used in CBCT technic such as Filtered Back Projection (FBP), Algebraic Reconstruction Technique (ART),

Simultaneous Iterative Reconstruction Technique (SIRT), Iterative Least-Squares Technique (ILST). FBP is an essential algorithm for practical CBCT due to its simplicity and parallel computing capability; FBP may produce a high-quality image if the step angle between two adjacent projections is small enough [5-8]. The quality of reconstructed images from FBP depends strongly on a spatial filter, which is applied to projections; a suitable filter can reduce artifact and increase contrast of imaging, while a bad filter can cause loss of imaging detail. Besides, the quality of reconstructed images also depends on the quality of FPD. To reduce the fluctuation of detectors in FPD and enhance the quality of projection data, we will have to implement FPD calibration regularly and apply a denoise filter to projections before performing filtered back projection. [9-11].

We used two sets of projection data for research in this paper. First, experiment projections, which are acquired from BKCT-01 – the first CBCT system was made in Vietnam. The second projection data was taken by MCNP simulation of BKCT-01 system. The reconstruction process is performed in two steps: the first step is processing images by apply denoise filtering to projection, and the second is the FBP step by apply spatial filter and back project. By assessing of reconstructed image, we can propose the best filters for BKCT-01 system.

## II. CONTENT

### a. Subject

The BKCT-01 system was manufactured at Hanoi University of Science and Technology (HUST) under national project KC.05.18/16-20. This is the first CBCT system was made in Vietnam. BKCT-01 can acquire and reconstruct 3D images of samples with

spatial resolution up to 100~200 $\mu\text{m}$ . BKCT-01's configuration is listed in table 1.

Table 1: Configuration of BKCT-01 system

<b>CBCT Gantry</b>	Source to Detector Distance (SDD): 993mm		
	Object to Detector Distance: ODD:		
	Sample rotation: from 0 to 360° with angle step is 0.5°		
<b>X-ray Source</b>	X-ray energy: 0 – 240kV		
	X-ray intensity: 0 – 3 mA		
	Spot size: 4 $\mu\text{m}$		
<b>Matrix detector FPD</b>		Normal mode	Binning mode
	Imaging size (pixel)	2944x2352	1472x1176
	Pixel pitch	49 $\mu\text{m}$	99 $\mu\text{m}$
	Resolution	10.1 LP/mm	5.0 LP/mm
	Framerate	Eight fps	32 fps
	Digital converter	14 bits	14 bits

To investigate the effect of filters on a reconstructed image's quality, we use a standard sample made of Aluminum. The shape of the sample is a tiered cylinder with an internal diameter of 28mm, the three-step cylinder has a thickness of 5 mm, and the diameter is 32, 34, and 36 mm, respectively. The standard sample has a machining tolerance of 50  $\mu\text{m}$ ; the sample's drawing is shown in figure 1.

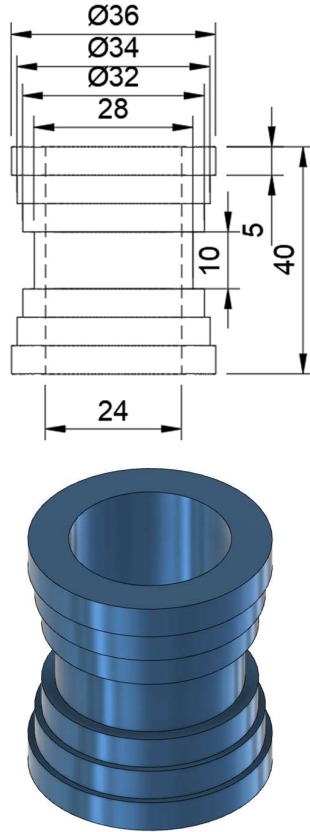


Figure 1: Dimension of Aluminum sample in mm

Because of tolerance of real sample and fluctuation of FPB itself can influence to result. Therefore, we simulated a CBCT system with a similar configuration with BKCT-01, and the simulating sample has the same size and material as the real one. Simulation software is MCNP; detail of simulation is not mentioned in this paper. Projection data in both experiment and simulation include 720 projections over 360° scanning angle; step angle is 0.5°. FPD in CBCT system working in normal mode with pixel size is 0.49 $\mu\text{m}$ . Projection datasets are preprocessed by applying denoise filters and then reconstructed using an FBP algorithm. By comparison results from the experiment and simulation, we can find the best filter for the reconstruction of BKCT-01 by using the FBP algorithm.

## b. Methods

As mentioned above, the projection datasets undergo two processing steps to obtain 3D reconstructed images: preprocessing and filtered back projection. In preprocessing step, each projection is applied denoise filter to reduce the statistical fluctuation of FPD and then convert the radiation intensity image to which is proportional to the integral of the sample's transmission coefficient. In the FBP step, projections are applied to the spatial filter and then back project to produce reconstructed images.

### • Denoising filters

In this paper, to eliminate the effect of FPD's statistical fluctuation, we will use two denoise filters: Median filter and Gaussian filter to apply to each projection. Median and Gaussian kernel is presented in table 2 [12].

Table 2: Median and Gaussian kernel

Filter	Kernel
Median filter	$M = \frac{1}{m \times n} \begin{bmatrix} 1 & 1 & 1 & \dots & 1 \\ 1 & 1 & 1 & \dots & 1 \\ \dots & \dots & \dots & \dots & \dots \\ 1 & 1 & 1 & \dots & 1 \end{bmatrix}$
Gaussian filter	$g(x, y) = ce^{-\frac{(x^2+y^2)}{2\sigma^2}}$

In which m and n are width and height of kernel matrix, respectively; c is constant and  $\sigma$  is the standard deviation of the Gaussian distribution.

### • Spatial filters

The spatial filter is the most crucial factor that decides the quality of the reconstructed image from the FBP algorithm. In this paper, we designed spatial filters in the frequency domain to reduce artifact; the filtering state is also done in the frequency domain, and then filtered projections are converted back to a

spatial domain for the back-projection state. Filtered back projection is described as below [13]:

$$g(t, s, z) = \int_0^{2\pi} \frac{D_{SO}^2}{(D_{SO} - s)^2} Q_{\beta} \left( \frac{D_{SO}t}{D_{SO} - s}, \frac{D_{SO}z}{D_{SO} - s} \right) d\beta \quad (1)$$

With:  $g(t, s, z)$  is a 3D reconstructed image of a sample in rotating coordinates  $(t, z, s)$ , which is interpolated from Cartesian coordinates  $(x, y, z)$ :

$$\begin{bmatrix} t \\ s \\ r \end{bmatrix} = \begin{bmatrix} 1 & 0 & 0 \\ 0 & \cos\gamma & \sin\gamma \\ 0 & -\sin\gamma & \cos\gamma \end{bmatrix} \begin{bmatrix} \cos\theta & \sin\theta & 0 \\ -\sin\theta & \cos\theta & 0 \\ 0 & 0 & 1 \end{bmatrix} \begin{bmatrix} x \\ y \\ z \end{bmatrix} \quad (2)$$

$D_{SO}$  is a distance from source to rotating center,  $\beta$  is a rotating angle of Object.

$Q_{\beta} \left( \frac{D_{SO}t}{D_{SO} - s}, \frac{D_{SO}z}{D_{SO} - s} \right)$  is a 2D projection of sample at rotated angle  $\beta$  that is calculated from equation (3) with  $R'_{\beta}$  is unfiltered projection, and  $h(t, s)$  is a spatial filtering.

$$Q_{\beta} \left( \frac{D_{SO}t}{D_{SO} - s}, \frac{D_{SO}z}{D_{SO} - s} \right) = R'_{\beta} \left( \frac{D_{SO}t}{D_{SO} - s}, \frac{D_{SO}z}{D_{SO} - s} \right) * \frac{1}{2} h(t, s) \quad (3)$$

We designed six spatial filters: Ram Lak, Shepp Logan, Cosine, Hann, Flattop, and Parzen for this research. These filters are applied to projections before the back projection state; by analysis and comparison result with six different filters, we can find the best filters for BKCT-01 system. Functions of filter is shown in table 2 [10,11,13].

Table 3: Spatial filtering function

Filter	Function
Ram Lak	$h_{ramp}(\omega) = \begin{cases}  \omega  & \text{if }  \omega  < W \\ 0 & \text{otherwise} \end{cases}$
Shepp Logan	$h_{shepp}(\omega) = \begin{cases}  \omega  \frac{\sin(\omega)}{\omega} & \text{if }  \omega  < W \\ 0 & \text{otherwise} \end{cases}$
Cosine	$h_{cosine}(\omega) = \cos\left(\frac{\pi n}{N} - \frac{\pi}{2}\right) \quad \text{if } 0 < n < N$
Hann	$h_{hann}(\omega) = 0.5 \left( 1 + \cos\left(\frac{2\pi n}{N}\right) \right) \quad \text{if } 0 \leq n \leq N$
Flattop	$h_{flattop}(\omega) = 0.21 - 0.41 \cos\left(\frac{2\pi\omega}{N-1}\right) + 0.27 \cos\left(\frac{4\pi\omega}{N-1}\right) - 0.08 \cos\left(\frac{6\pi\omega}{N-1}\right) + 0.006 \cos\left(\frac{8\pi\omega}{N-1}\right) \quad \text{if } 0 \leq n \leq N$
Parzen	$h_{parzen}(\omega) = \begin{cases} 1 - 6\left(\frac{ \omega }{N/2}\right)^2 + 6\left(\frac{ \omega }{N/2}\right)^3 & \text{if } 0 \leq  \omega  \leq (N-1)/4 \\ 2\left(1 - \frac{ \omega }{N/2}\right)^3 & \text{if } (N-1)/4 \leq  \omega  \leq (N-1)/2 \end{cases}$

In which:  $W$  is limiting frequency of sampling process:  $W = \frac{1}{2t}$  with  $t$  is time interval so call pixel size

of FPD,  $t = 49\mu\text{m}$ ,  $N$  is number pixel of FPD along filtering line. From the FPD parameters, we can

design a natural response of six spatial filters for the BKCT-01 system, as shown in figure 2.

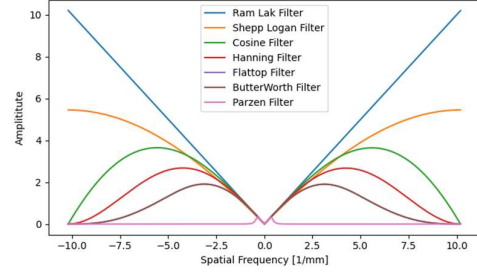


Figure 2: Response of six different spatial filters is used in this paper

#### • Modulation transfer function (MTF)

MTF of an imaging system is a measurement of its ability to transfer contrasts at a particular resolution from the Object to the image. MTF can show the limiting spatial resolution of the reconstructed image; for example, figure 3 shows the limiting spatial resolution at 10% modulation. MTF can be achieved by taking the Fourier transform of line spread function LSF along the edge from a region of interest (ROI) as follows [2].

$$MTF = \left| \int_{-\infty}^{\infty} LSF(x) e^{-2\pi i f x} dx \right| \quad (4)$$

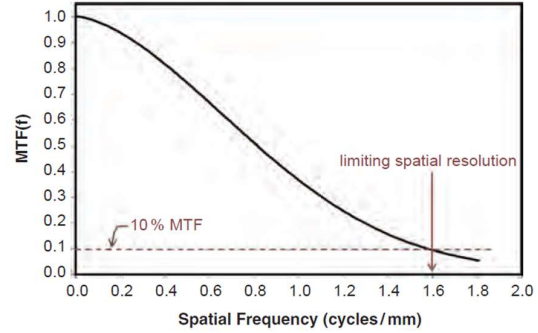


Figure 3: Response of MTF

#### • Signal to Noise Ratio (SNR) and Contrast to Noise Ratio (CNR)

We used the SNR and CNR ratio to measure the level of noise on ROI. MTF is a useful metric for describing an image's quality; the higher SNR and CNR mean the better quality. The SNR and CNR are given by [2]:

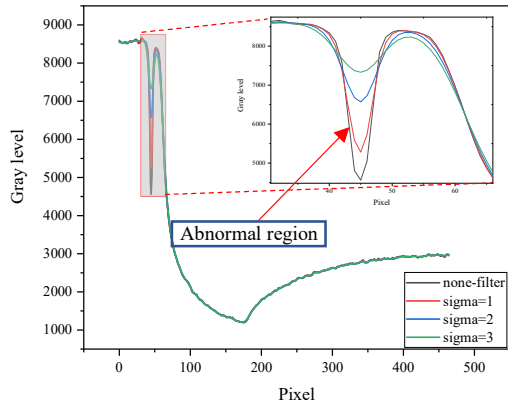
$$SNR = \frac{\sum_i (x_i - \overline{x_{bg}})}{\sigma_{bg}} \quad (5)$$

With:  $x_i$  is the gray value of ROI signal,  $\overline{x_{bg}}$  is a mean background and  $\sigma_{bg}$  is a standard deviation of noise.

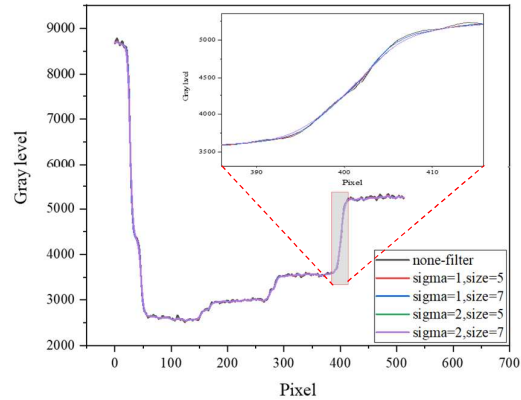
$$CNR = \frac{(\overline{x_s} - \overline{x_{bg}})}{\sigma_{bg}} \quad (6)$$

With: is an average gray value of ROI signal,  $\bar{x}_{bg}$  is a mean background and  $\sigma_{bg}$  is a standard deviation of noise.

**c. Result**  
 • *Quality of projections*

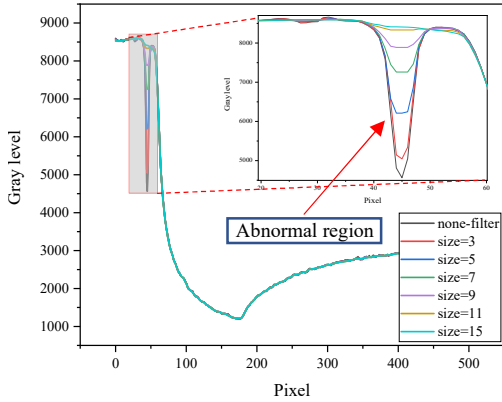


a) Vertical slice

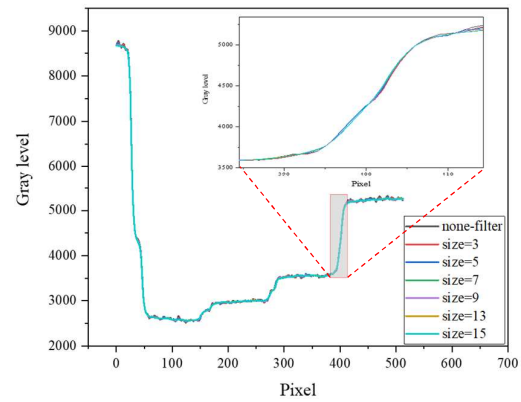


b) Horizontal slice

Figure 4: Horizontal and vertical slices of the Object using Gaussian filter for Preprocessing

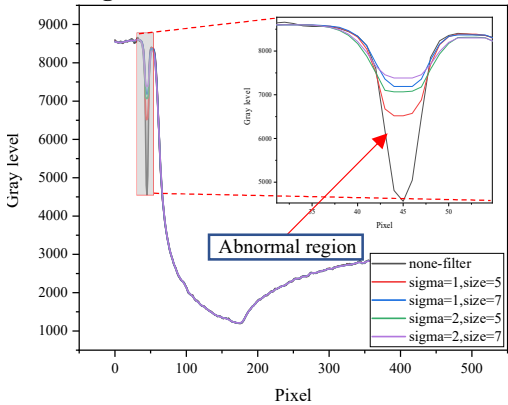


a) Vertical slice

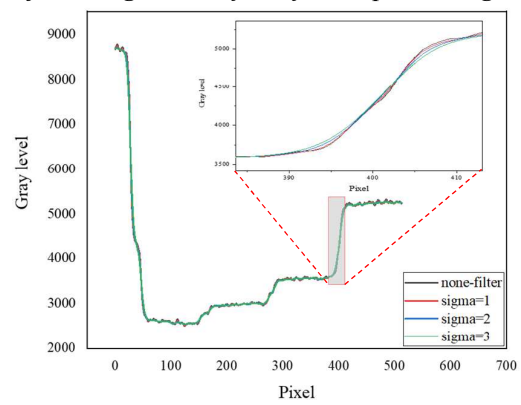


b) Horizontal slice

Figure 5: Horizontal and vertical slices of the Object using Median filter for Preprocessing



a) Vertical slice



b) Horizontal slice

Figure 6: Horizontal and vertical slices of the Object using both Gaussian and Median filter for Preprocessing

Figures 4a, 5a, and 6a show a slice of projection that has abnormal areas. The irregular area is a negative peak at the position of column 45 in the image matrix. The gray level here drops to the very low level of 4500, without a denoise filter. After applying filters, this peak becomes shorter; as we can see from the figures above, the larger the filter

coefficients, the better remove the noise signal. Figures 4a, 5a, and 6a show the effect of kernel size on image sharpness. When we increase the filter's kernel size, the edge of the image becomes more inclined, and this effect will reduce the spatial resolution of an image.

Table 4 shows the processing time for the denoise filter when applying to projection is shown, the processing time from 0.02 to 0.031 seconds for the Gaussian filter, and from 0.1 to 2.2s for the median filter. The Median processing time is much larger than the Gaussian filter, and this time also increases with the filtering kernel size.

Table 4: Time to filter noise for one projection

Filter		Time (s) per projection
Gaussian	Sigma = 1	0.02
	Sigma = 2	0.03
	Sigma = 3	0.03
Median	S = 3x3	0.10
	S = 5x5	0.32
	S = 7x7	0.59
	S = 9x9	0.92
	S = 15x15	2.20

Since the quality of projections itself will affect the quality of reconstructed images, we must also evaluate the noise level of projections using CNR and

SNR values. The results are presented in Table 5. We can see that when the filter's kernel size is increased, CNR and SNR are becoming more significant.

Table 5: Results of the calculation of CNR and SNR ratio for the projection after filtering

Filter	CNR	SNR	
Gaussian	Sigma = 1	147.71	20.90×10 <sup>6</sup>
	Sigma = 2	162.24	23.68×10 <sup>6</sup>
	Sigma = 3	180.20	24.57×10 <sup>6</sup>
Median	S = 5x5	153.41	21.91×10 <sup>6</sup>
	S = 7x7	160.83	23.38×10 <sup>6</sup>
	S = 9x9	166.65	24.77×10 <sup>6</sup>
	S = 11x11	171.40	26.17×10 <sup>6</sup>
	S = 15x15	180.11	0.14×10 <sup>6</sup>
Combine	Sigma = 1, s=5x5	157.61	22.84×10 <sup>6</sup>
	Sigma = 1, s=7x7	163.25	23.93×10 <sup>6</sup>
	Sigma = 2, s=5x5	165.55	24.60×10 <sup>6</sup>
	Sigma = 2, s=7x7	168.45	25.32×10 <sup>6</sup>

- *Quality of reconstructed image*

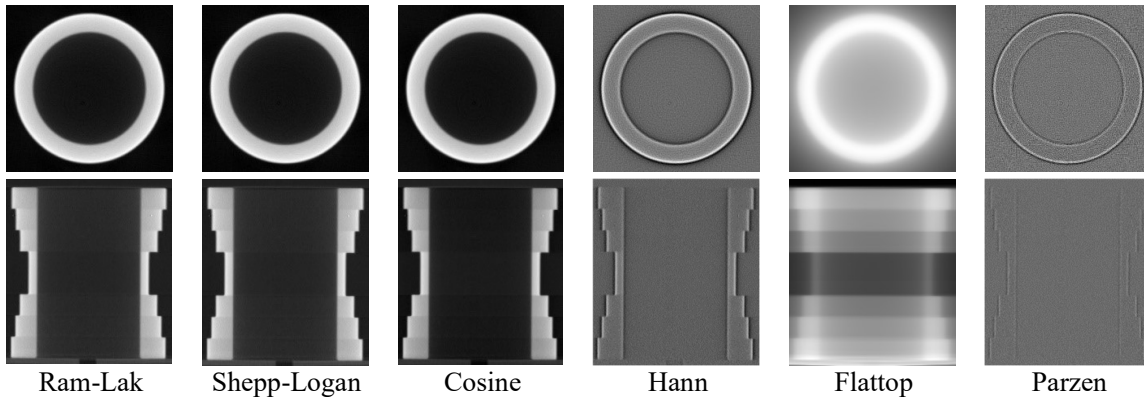


Figure 7: Object's reconstructed image with experimental projections

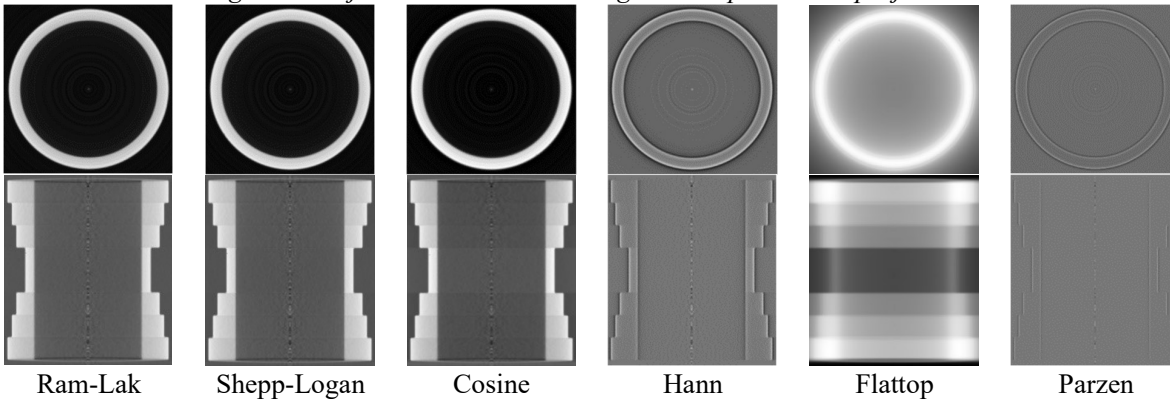


Figure 8: Object's reconstructed image with simulating projections

Figure 7 and Figure 8 show the horizontal and vertical slices of the reconstructed image. The actual object size does not change when using different types

of filters. We can see that Ram-Lak, Shepp-Logan, and cosine filter generate similar results by observing with the naked eye. Hann and Parzen make a sharper

image (detect edge only), while the result achieved by apply the Flattop filter is blurry. For further analysis, we plot a 1D curve of vertical-horizontal, as shown in Figure 8. It shows that cosine makes a base level of signal drops close to zero (reduction of DC shift), better than Ram-Lak and Shepp-Logan do. In addition, when evaluating with SNR and CNR ratios

(result in Table 6), Ram-Lak, Shepp-Logan, and Cosine filter gave relatively large values of CNR and SNR among the six filters used. While the Hann, Flattop, and Parzen filter have a meager CNR ratio, it can be seen clearly in the image with almost indistinguishable details in the area with the Object; only the edges are visible.



Figure 8: Vertical and horizontal slice from Object's reconstructed image

Table 6: Results of calculation of CNR and SNR ratio for reconstructed image

Filter		Ram-Lak	Shepp Logan	Cosine	Hann	Flattop	Parzen
CNR	Simulation	13.17	13.20	15.42	2.69	1.27	0.61
	Experiment	33.96	33.99	39.52	9.92	1.40	2.62
SNR	Simulation	$1.86 \times 10^6$	$1.89 \times 10^6$	$2.20 \times 10^6$	$3.85 \times 10^5$	$1.83 \times 10^5$	$8.78 \times 10^4$
	Experiment	$4.73 \times 10^6$	$4.73 \times 10^6$	$5.50 \times 10^6$	$1.38 \times 10^5$	$1.95 \times 10^5$	$3.65 \times 10^5$

- **Modulation transfer function (MTF)**

Measure the intensity of reconstructed along the edge of a sample. We can present the LSF of the picture.

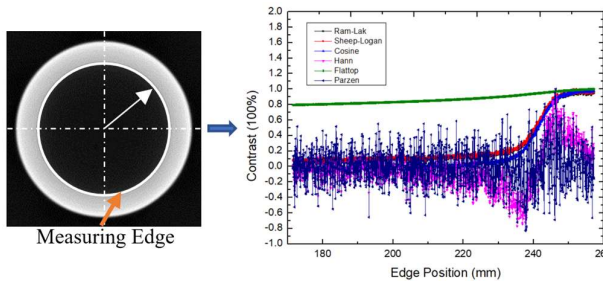


Figure 9: LSF of reconstructed slide with difference filters

By taking the Fourier transform of Line Spread Function, we can measure Modulate Transfer Function of reconstructed image when applying different filter types.

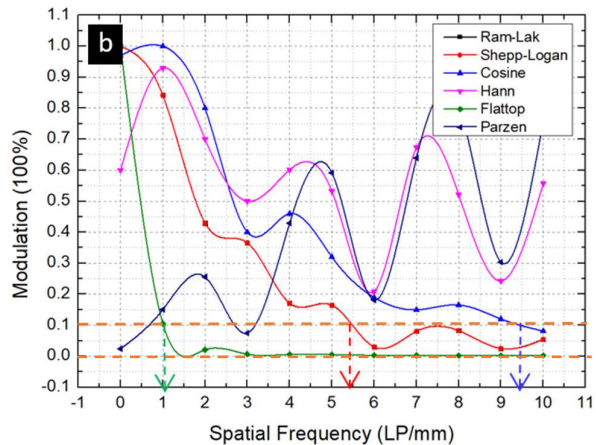
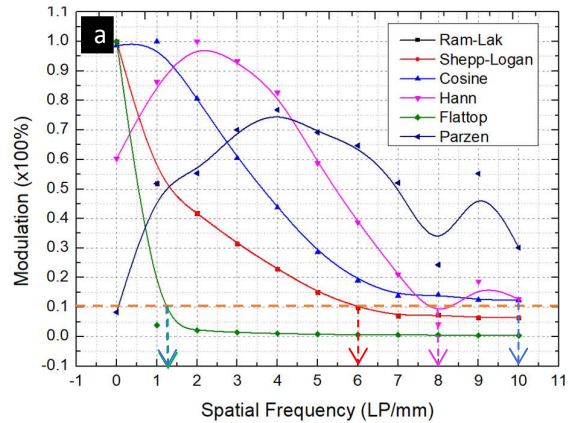


Figure 10: Fitting function of MTF of reconstructed image by applying six difference filters; (a): result from real sample, (b): result from simulating sample

As we can see from the figure, the contrast of result from Flattop filter quickly drop below 10% of modulation at around 1 LP/mm; Hann and Flattop caused low modulation at low frequency and then oscillated when frequency increases. Ram-Lak and Shepp-Logan have similar responses with limiting spatial resolution, which is 6 and 5.5 LP/mm for results from real sample and simulating sample, respectively. Cosine filter has limiting spatial resolution around 10LP/mm for both actual sample and simulating one.

- **Calculation of Object's dimension**

To calculate the sample's dimension in both experimental and simulated cases, we detect a contour of Object in the reconstructed image, then measure these contours; results are shown in Table 7. The calculated values show that the diameter of the Object is relatively accurate compared with the fabrication size of the specimen. The difference is less than the value of 2 pixels, which is less than  $100\mu\text{m}$ .

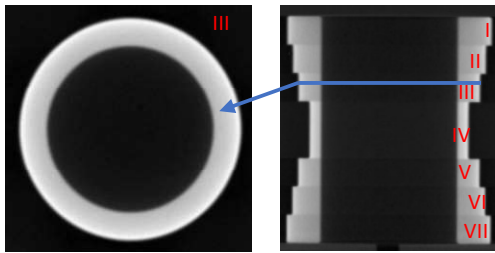


Figure 11: Mark the dimension of Object

Table 7: Results of calculating reconstructed Object's dimension

Slice	Actual size (mm)	Measuring size from reconstructed image (mm)	
		Experimental Sample	Simulating Sample
I	36 ( $\pm 0.05$ )	35.929 $\pm$ 0.081	35.988 $\pm$ 0.077
II	34 ( $\pm 0.05$ )	33.964 $\pm$ 0.073	33.918 $\pm$ 0.075
III	32 ( $\pm 0.05$ )	32.000 $\pm$ 0.075	31.962 $\pm$ 0.075
IV	28 ( $\pm 0.05$ )	28.084 $\pm$ 0.075	28.060 $\pm$ 0.078
V	32 ( $\pm 0.05$ )	32.009 $\pm$ 0.080	31.962 $\pm$ 0.075
VI	34 ( $\pm 0.05$ )	34.059 $\pm$ 0.068	33.913 $\pm$ 0.080
VII	36 ( $\pm 0.05$ )	35.926 $\pm$ 0.077	35.988 $\pm$ 0.075

#### d. Discussion

Because of the detector system's instability, we have detected some abnormal regions in the acquired projection; it can be seen in Figure 4a and Figure 5b. The use of Gaussian and Median filters can help solve this problem. The larger the filter coefficients, the better the removal of the anomalous signal. The median function with a filter coefficient (Kernel matrix size) of 15x15 can reduce the signal's noise level better than the Gaussian filter. However, the problem is that too much filtering can lose information of the image, making the edge of the

Object in the projections even more slopping, as can be seen in Figure 4b, 5b, and 6b. Therefore, the selection of a large filter coefficient needs to be carefully considered. Here we also find that using the Median filter requires a greater computation time than the Gaussian filter (shown in Table 4). Therefore, we should not choose a Median filter with a large size such as 11x11 or 15x15, because when dealing with large number projections, the filtering process will take much time and then reduce computing performance.

The projections' quality will also affect the reconstructed image quality, so here we also further evaluate the Contrast to Noise and Signal to Noise ratio from Equation 5 and 6 given above. Increasing the filter coefficient will give better quality. However, as mentioned above, we cannot arbitrarily increase the filter coefficient because it will lose the edges of images' sharpness. Furthermore, with the resolution requirement, when using the filters, the image's spatial resolution will be decreased. The Median filter with a Kernel size of 7x7 will have a resolution of about 0.2mm while filtering with a Kernel size of 3x3 equivalent to a resolution of 0.05mm is not enough. Therefore, we propose a filtration scheme with a Sigma coefficient equal to 1 or 2 and use Median with Kernel size of 5x5. The set of chosen filters can be expected to achieve results with a resolution around 0.1mm.

The spatial resolution of the reconstructed image is measured in figure 10; the response of Ram-Lak, Shepp-Logan, cosine, Flattop in both experimental and simulated sampling is quite similar. In simulating the sample, the curve of these filters is a little bit oscillated of high frequency due to high-frequency noise, which is caused by statistical fluctuation when simulation time of MCNP is not high enough. Reconstruction from projections of simulating sample will lead to spatial resolution of simulation results is slightly smaller than from experiment. Hann and Flattop filters have a smoother response at high frequency; therefore, they fluctuate strongly when the frequency is increased and may not be used in case of simulating sample.

Table 7 shows the sample's dimension, which is calculated from the reconstructed image with a cosine filter; maximum machining tolerances of the real sample is 0.05mm; tolerance does not appear in the simulated sample. We could see that the maximum error of dimension does not exceed 0.1mm; this corresponds to limiting spatial resolution, which is measured in figure 10.

### III. CONCLUSION

In this paper, some denoise filters and spatial filters are used to evaluate the reconstructed image's quality from the cone-beam CT system. The results show that we should first apply the denoise filter for all projections in the preprocessing step because noise appears in projections acquired in both simulation and experiment. The most suitable filter for the denoising process is a mix of Gaussian and Median with the right kernel size. If we want to eliminate high-frequency noise in projections, we need a larger filter, but this will reduce the reconstructed image's sharpening. The median filter has a better response than the Gaussian filter, but the Median's processing time is much slower than Gaussian. Therefore, the combination of these two filters is needed.

The spatial filter has a significant effect on the quality of the reconstructed image. From the results, we can see that the reconstructed image has the highest spatial resolution by applying a cosine filter. Limiting the spatial resolution of reconstructed data for both real simulation samples is around 10LP/mm. It means that by applying a cosine filter, we could distinguish two points with the smallest distance is 0.1mm on the reconstructed image. Ram-Lak and Shepp-Logan filters have similar response with a limiting resolution is around 6LP/mm. Hann and Parzen make images with low contrast at low frequency and increase at higher one, while Flattop makes image drop contrast quickly when frequency increases. Therefore, we will choose a cosine filter to achieve an image with high resolution and a wide range of contrast (having full information of the reconstructed sample). Nevertheless, if we want to obtain a high frequency of images only, we only want to see the edge of the Object in an image; for example, we should use a Hann filter in a segmentation application.

By evaluation of the effect of filter types on quality of reconstructed image when using FBP algorithm on CBCT system, we chose a suitable filter for reconstruction of BKCT-01 system. The system can archive a good quality of the reconstructed image and then accurately measure the sampling object's dimension by Using the right set of filters.

### ACKNOWLEDGMENTS

This research is supported by KC.05.18/16-20 Project of Ministry of Science and Technology and Vietnam Atomic Energy Institute via VINATOM-HPC system.

### REFERENCES

1. Shaithya Kailash "CBCT-Cone Beam Computed Tomography," Journal of Academy of Dental Education, 9-15.
2. Jerrold T. Bushberg, J. Anthony Seibert, Edwin M. Leidholdt JR, John M. Boone, "The essential physics of medical imaging", 3rd edition, Lippincott William & Wilkins, 2012, p70-72, 91-92, 312-318.
3. J.P. Kruth, M. Bartscher, S. Carmignato, L. De Chiffre, A. Weckenmann, "Computed Tomography for dimensional metrology", CIRP Annals – Manufacturing Technology 60 (2011),655-677.
4. L. De Chiffre, S. Carmignato, J.P. Kruth, R. Schmitt, A. Weckenmann, "Industrial application of Computed Tomography", CIRP Annals – Manufacturing Technology 63 (2014),655-677.
5. Jia, X., Dong, B., Lou, Y., & Jiang, S. B. (2011), "GPU-based iterative cone-beam CT reconstruction using tight frame regularization", *Physics in Medicine & Biology*, 56(13), 3787.
6. Hsieh, J., Nett, B., Yu, Z., Sauer, K., Thibault, J. B., & Bouman, C. A. (2013), "Recent advances in CT image reconstruction", *Current Radiology Reports*, 1(1), 39-51.
7. Pack, J. D., Noo, F., & Clackdoyle, R. (2005). "Cone-beam reconstruction using the back projection of locally filtered projections". *IEEE Transactions on Medical Imaging*, 24(1), 70-85.
8. Scherl, H., Koerner, M., Hofmann, H., Eckert, W., Kowarschik, M., & Hornegger, J. (2007, March). Implementation of the FDK algorithm for cone-beam CT on the cell broadband engine architecture. In *Medical Imaging 2007: Physics of Medical Imaging* (Vol. 6510, p. 651058). International Society for Optics and Photonics.
9. Mark Plachtovics, Janos Goczan, Katalin Nagy, "The effect of calibration and detector temperature on the reconstructed cone beam computed tomography image quality: a study for the workflow of the iCAT Classic equipment", *Oral Surgery, Oral Medicine, Oral Pathology and Oral Radiology*, Vol 119, Issue 4 (2015), p-473-480.
10. Yuuki Houno, Toshimitsu Hishikawa, Ken-ichi Gotoh, Munetaka Naitoh, Akio Mitani, Toshihide Noguchi, Eiichiro Arijii, Yoshie Kodera, "Optimizing the reconstruction filter in cone-beam CT to improve periodontal ligament space

- visualization: An in vitro study*”, *Imaging Science Density*, 2017 Sep;47(3):199-207.
11. Julia F. Barnet, Nicholas Keat, “*Artifact in CT: Recognition and Avoidance*”, *Radio graphic* (2004), 24, p1679-1691.
  12. Linda G. Shapiro, George Stockman, “*Computer Vision*”, University of Washington, 2000, p154-155,168
  13. Avinash C. Kak, Malcolm Slaney, “*Principle of Computerized Tomographic Imaging*”, SIAM, 1988, p71-74,104-107.